Journal of Medicinal Chemistry

Article

pubs.acs.org/jmc

Peroxisome Proliferator-Activated Receptors (PPARs) Have Multiple Binding Points That Accommodate Ligands in Various Conformations: Phenylpropanoic Acid-Type PPAR Ligands Bind to PPAR in Different Conformations, Depending on the Subtype

Naoyuki Kuwabara,[†,‡] Takuji Oyama,[†,§] Daisuke Tomioka,[∥] Masao Ohashi,[⊥] Junn Yanagisawa,[▽] Toshiyuki Shimizu,[‡] and Hiroyuki Miyachi*[,⊥]

[‡]Graduate School of Pharmaceutical Sciences, Faculty of Pharmaceutical Sciences, The University of Tokyo, 7-3-1 Hongo, Bunkyo-ku, Tokyo 113-0033, Japan

[§]Institute for Protein Research, Osaka University, 6-2-3 Furuedai, Suita, Osaka 565-0874, Japan

[∥]Graduate School of Nanobioscience, Yokohama City University, 1-7-29 Suehiro-cho, Tsurumi-ku, Yokohama 230-0045, Japan

[⊥]Graduate School of Medicine, Dentistry and Pharmaceutical Sciences, Okayama University, 1-1-1 Tsushima-Naka, Kita-ku, Okayama 700-8530, Japan

[▽]Graduate School of Life and Environmental Sciences, University of Tsukuba, Tsukuba Science City, Ibaraki 305-8577, Japan

ABSTRACT: Human peroxisome proliferator-activated receptors (hPPARs) are ligand-dependent transcription factors that control various biological responses, and there are three subtypes: hPPARα, hPPARδ, and hPPARγ. We report here that α-substituted phenylpropanoic acid-type hPPAR agonists with similar structure bind to the hPPAR ligand binding domain (LBD) in different conformations, depending on the receptor subtype. These results might indicate that hPPAR ligand binding pockets have multiple binding points that can be utilized to accommodate structurally flexible hPPAR ligands.

1. INTRODUCTION

The nuclear hormone receptors (NRs), which comprises 48 members in humans, form a superfamily of ligand-dependent transcription factors that control diverse biological functions, including reproduction, development, homeostasis, and immune function.[1] Among them, much attention has been focused on the human peroxisome proliferator-activated receptors (hPPARs), mainly because of their pleiotropic roles in glucose, lipid, and lipoprotein homeostasis.[2] hPPARs are activated by endogenous saturated and unsaturated fatty acids, their metabolites, and synthetic ligands.[3] The three subtypes, hPPARα, hPPARδ, and hPPARγ, are differentially expressed in a tissue-specific manner.[4] hPPARs were initially recognized as therapeutic targets for the development of drugs to treat metabolic disorders, such as diabetes and dyslipidemia.[5] But, the range of the therapeutic potential for hPPAR ligands is currently expanding well beyond lipid, lipoprotein, and glucose homeostasis, and hPPAR biology and pharmacology are attracting enormous interest.[6−10]

In the design of new ligands (agonists or antagonists), X-ray crystallographic analysis of ligands complexed with the target protein is a powerful approach to understand the binding mode of ligands to the target protein, and also to provide clues for improving the binding affinity and selectivity. Since the first report of the crystal structure of the hPPARγ ligand binding domain (LBD) complexed with the antidiabetic drug rosiglitazone,[11] many atomic structures of hPPAR LBD−ligand complexes with a variety of natural fatty acids and synthetic compounds have been reported.[12]

We have been engaged in structural development studies of subtype-selective hPPAR ligands, and we have successfully designed and synthesized a series of substituted phenylpropanoic acid human hPPARα-selective agonists,[13] a hPPARα/δ dual agonist (TIPP-401 (**1**)),[14] a hPPARδ-selective agonist (TIPP-204 (**2**)),[15] a hPPAR $\alpha/\delta/\gamma$ pan agonist (TIPP-703 (**3**)),[16] and hPPARγ-selective agonists (Table 1).[17] We also have reported the binding modes of some of our compounds complexed with hPPAR subtypes, i.e., hPPARδ LBD−**1** complex, hPPARδ LBD−**2** complex, hPPARα LBD−**3** complex, hPPARγ LBD−**3** complex, and so on.[18−20] These structural biology studies prompted us to examine the structural basis for the hPPARδ−selective agonistic activity of **2**, in contrast to the agonistic activity of **3** toward all hPPAR subtypes. Therefore, we performed further X-ray crystallographic analysis of our compounds complexed with LBDs of hPPAR subtypes.

In this paper, we present further structural biology results for our phenylpropanoic acid hPPARα/δ dual agonist (**4**) complexed with hPPARδ LBD, hPPARα/δ dual agonist (**5**) complexed with hPPARγ LBD, and hPPARγ/δ dual agonist (**6**) complexed with hPPARγ LBD (Table 1). Interestingly, the present series of hPPAR agonists are all structurally similar, but they bind to hPPARγ LBD in distinct conformations, as compared to the binding conformations with the other two hPPAR subtypes.

Received: October 21, 2011
Published: December 19, 2011

Table 1. Chemical Structures and hPPARs Transactivation Activities of the Present Series of Compounds

compd.		EC_{50} (nM) PPARγ	PPARα	PPARδ
1	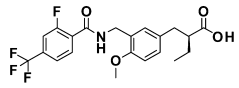	1900	10	12
2	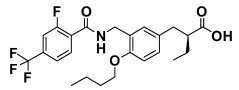	1400	24	0.72
3	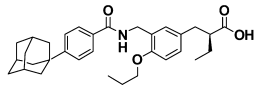	43	61	120
4	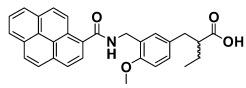	ia	12	43
5	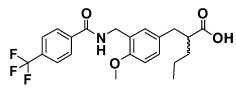	3600	63	120
6	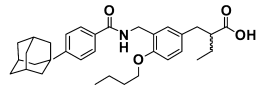	58	1400	190

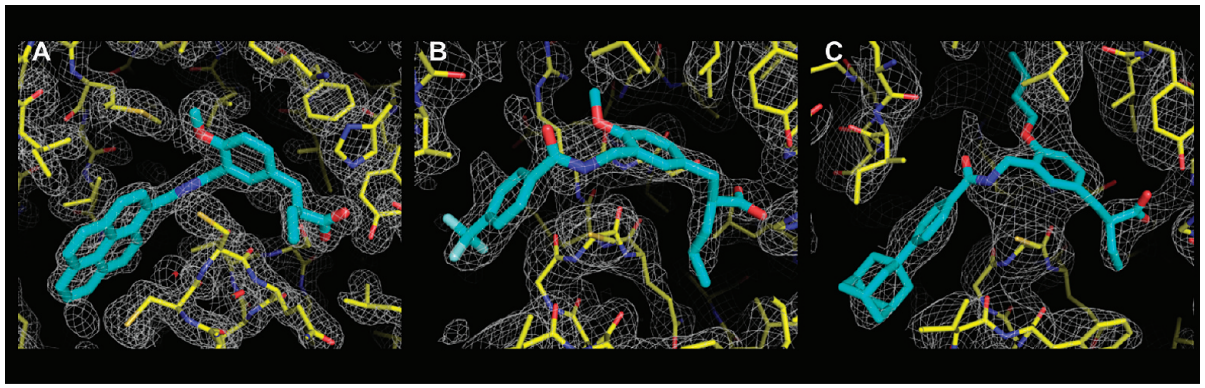

Figure 1. Close-up views of the OMIT Fo-Fc electron-density maps (contoured at 2.2 Å) of (A) hPPARα LBD−**4** complex, (B) hPPARγ LBD−**5** complex, and (C) PPARγ LBD−**6** complex.

2. RESULTS AND DISCUSSION

2.1. Chemistry. Compounds **4**, **5**, and **6** have already been synthesized, and the physicochemical properties of **4** were reported.[14] Compounds **4**−**6** were used as racemates for the X-ray crystallographic studies, but the compounds cocrystallized with hPPARα LBD and hPPARγ LBD were all of *S* configuration, based on their electron-density maps (Figure 1). These results are consistent with our previous finding that the hPPAR transactivation activity of the present series of α-alkylphenylpropanoic acid derivatives resides mainly in the *S* enantiomer.[13−17]

2.2. Expression, Purification, and Crystallization. The recombinant ligand-binding domain (LBD) of hPPARγ (residues 203−477) was expressed as an *N*-terminal His-tagged protein in *E. coli* BL21 (DE3), using the pET28a vector (Novagen). The protein was purified by means of several steps of column chromatography. Apo PPARγ LBD crystals were soaked in ligand solution for two or three weeks. The crystal of hPPARα LBD−**4** belongs to space group $p2_1$, and those of hPPARγ LBD−**5** and hPPARγ LBD−**6** belong to space group *C*2. Determination of the hPPARα LBD−**4** cocrystal structure was performed as described previously, including protein purification, crystal growth, and structural refinement.[18]

2.3. Diffraction Data Collection. The diffraction data for the hPPARα LBD complex with **4** were collected on BL38B1 at SPring-8 (Harima, Japan) and were processed using HKL-2000. The diffraction data for the hPPARγ LBD complex with **5** or **6** were collected on BL5A or BL17A at PF (Tsukuba, Japan) using ADSC Quantum 315 or 270 CCD. Diffraction data were processed with HKL2000.[16]

2.4. Structure Analysis and Refinement. The structure of the hPPARα LBD complex with **4** was solved by the molecular-replacement method with the program *CNS*[21] using the previously reported structures as probes. The correctly positioned molecules were refined with *CNS* and *O*.[22] The initial atomic model of **4** was built using *MOE* (Ryoka Systems Inc.), and topology and parameter files for the refinement were generated by the *HIC-Up* server.[23]

The structure of hPPARγ LBD was solved by the molecular replacement method using Molrep. The Apo PPARγ LBD structure (PDB code 1PRG) was used as a search model and refined with Refmac5. The crystallographic data and data collection statistics of all the crystals are provided in Table 2.

2.5. Comparison of the Three-Dimensional Structures of the hPPAR LBDs. It is well established that PPAR LBDs have similar structural folds. Each of the hPPAR LBDs folds into a three-layered sandwich structure composed mainly of α-helices, as also observed in the case of the nuclear receptor LBDs (Figure 2). The loop between helices H2′ and H3, the so-called omega loop,[24] is poorly defined, probably due to thermal mobility. hPPAR has a large Y-shaped ligand binding pocket consisting of Y1, Y2, and Y3 arms.[11] The Y1 arm extends through the space between H3, H4, and H2. The Y2 arm is situated between H3 and the β-sheet. The Y3 arm extends through the space between H12, H4, and H10/H11. The Y3 arm forms the only substantially polar hPPAR cavity, while the Y1 and Y2 arms are mainly hydrophobic. Most of the natural and synthetic ligands of hPPARs are reported to fit into these three arms. For example, the naturally occurring unsaturated fatty acid eicosapentaenoic acid (EPA), which lowers triglyceride levels and enhances insulin sensitivity, binds

dx.doi.org/10.1021/jm2014293 | J. Med. Chem. 2012, 55, 893−902

Table 2. Crystallographic Data and Refinement Statistics[a]

	hPPARα LBD−4	hPPARγ LBD−5	hPPARγ LBD−6
resolution (Å)	1.75	2.2	2.6
space group	*p* 21	*C* 2	*C* 2
cell constant			
a (Å)	44.37	92.97	93.15
b (Å)	61.3	60.49	60.61
c (Å)	53.18	117.96	118.77
β (deg)	106.95	103.35	103.79
completeness (%)	98.9	97.98	83.49
no. of reflections	27254	29325	15775
R merge			
R/*R* free	21.3/24.6	20.6/24.7	21.2/28.0
rmsd bond length	0.006	0.01	0.013
rmsd bond angle	1.100	1.069	1.311
PDB code	3VI8	3VJH	3VJI

[a]Values in parentheses are for the last shell.

to the hPPARδ LBD in two distinct conformations.[25] One is a "tail-up" conformation, such that the acidic head part of the EPA molecule is located in the Y1 arm, while the hydrophobic tail part of it is buried in the upper Y3 arm (Figure 2B). The other is a "tail-down" conformation, such that the acidic head part of the EPA molecule is again located in the Y1 arm, but the hydrophobic tail part of it is buried in the lower Y2 arm (Figure 2C). In the case of the potent and hPPARδ−selective fibrate-type agonist GW-2433 (2-(4-(3-(1-(2-chloro-6-fluorophenethyl)-3-(2,3-dichlorophenyl)ureido)propyl)phenoxy)-2-methylpropanoic acid), the two urea substituents (the 2,3-dichlorophenyl group and 2-chloro-6-fluorophenylethyl group) project into the Y2 arm and Y3 arm, respectively, and form hydrophobic interactions.[25]

2.6. Detailed Comparison of the Binding Modes of α-Alkylphenylpropanoic Acid Derivatives to PPAR LBDs. We solved the X-ray crystallographic structures of hPPARδ/α−dual agonist (**1**) and PPARδ−selective agonist (**2**) complexed with hPPARδ LBD at 3.0 Å and 2.6 Å resolutions, respectively. The results are depicted in Figure 3 (D and E). As we had expected, the acidic head part of both **1** and **2**, i.e., the α-ethylpropanoic acid moiety, was buried in the Y1 arm, forming a hydrogen bonding network to His323, His449, and Tyr473. The hydrophobic tail part of both **1** and **2** is buried in the more hydrophobic Y2 arm of hPPARδ LBD (Figure 3C and G). We had speculated that the alkoxy groups of **1** and **2** on the central benzene ring would both interact with the Y3 arm (Figure 3G). However, detailed structural analysis clearly indicated that both

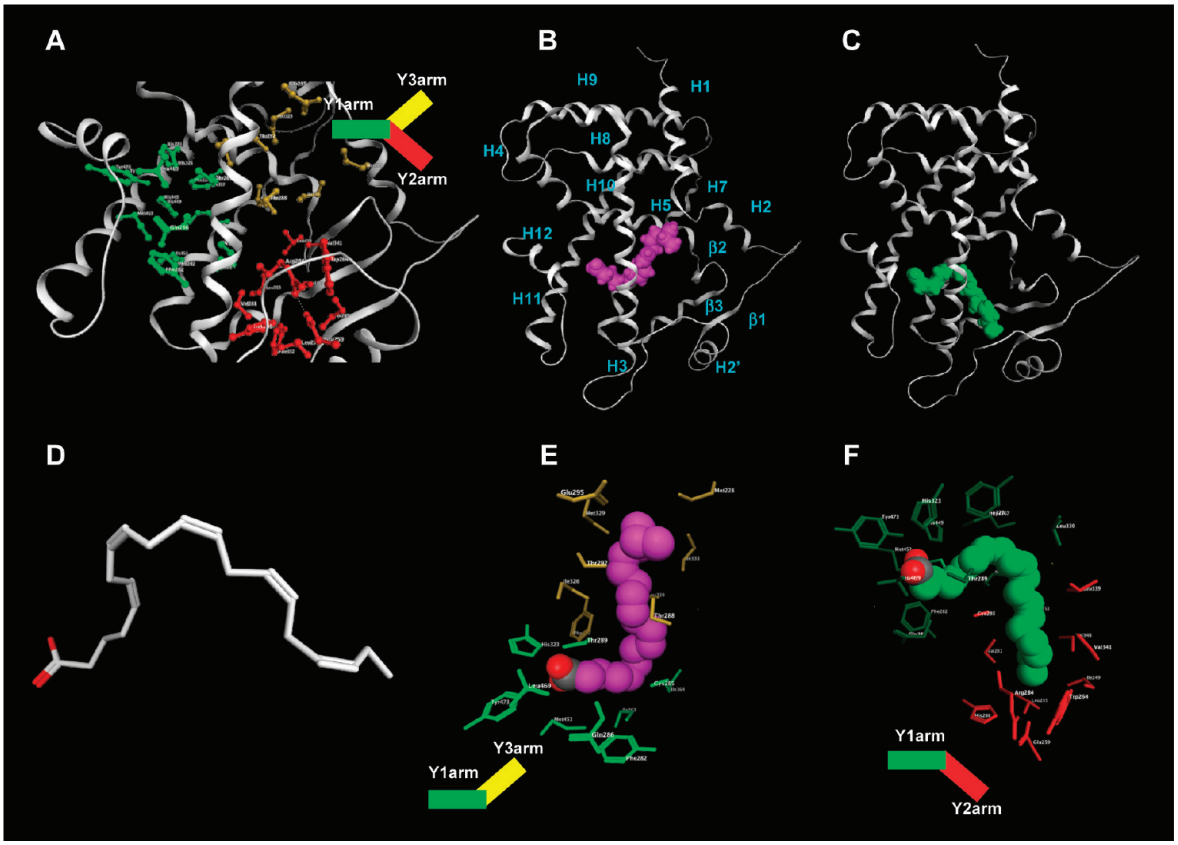

Figure 2. Crystal structures of hPPARs LBD−eicosapentaenoic acid (EPA) complexes (PDB: 3GWX). (A) Zoomed view of the Y-shaped ligand-binding pocket of hPPARd LBD. Protein is represented as a white ribbon model, and the Y1, Y2, and Y3 arm amino acids are depicted as green, red, and yellow ball-and-stick models, respectively. (B) Whole structure of the hPPARδ LBD−tail-up mode EPA complex. The ligand is depicted as magenta space-filling models. The numbering of the second structure is also depicted. The nomenclature of the helices is based on the RXR-α crystal structure. (C) Whole structure of the hPPARδ LBD−tail-down mode EPA complex. The ligand is depicted as green space-filling models. (D) Bound EPA structure. The ligand is depicted as a cylinder model. (E) Zoomed view of the binding mode of tail-up EPA in the Y1−Y3 arms. The Y1 arm amino acids and Y3 arm amino acids are depicted as green and yellow cylinders, respectively. EPA is depicted as a space-filling model. (F) Zoomed view of the binding mode of tail-down EPA in the Y1−Y2 arms. The Y1 arm amino acids and Y2 arm amino acids are depicted as green and red cylinders, respectively. EPA is depicted as a space-filling model.

dx.doi.org/10.1021/jm2014293 | J. Med. Chem. 2012, 55, 893−902

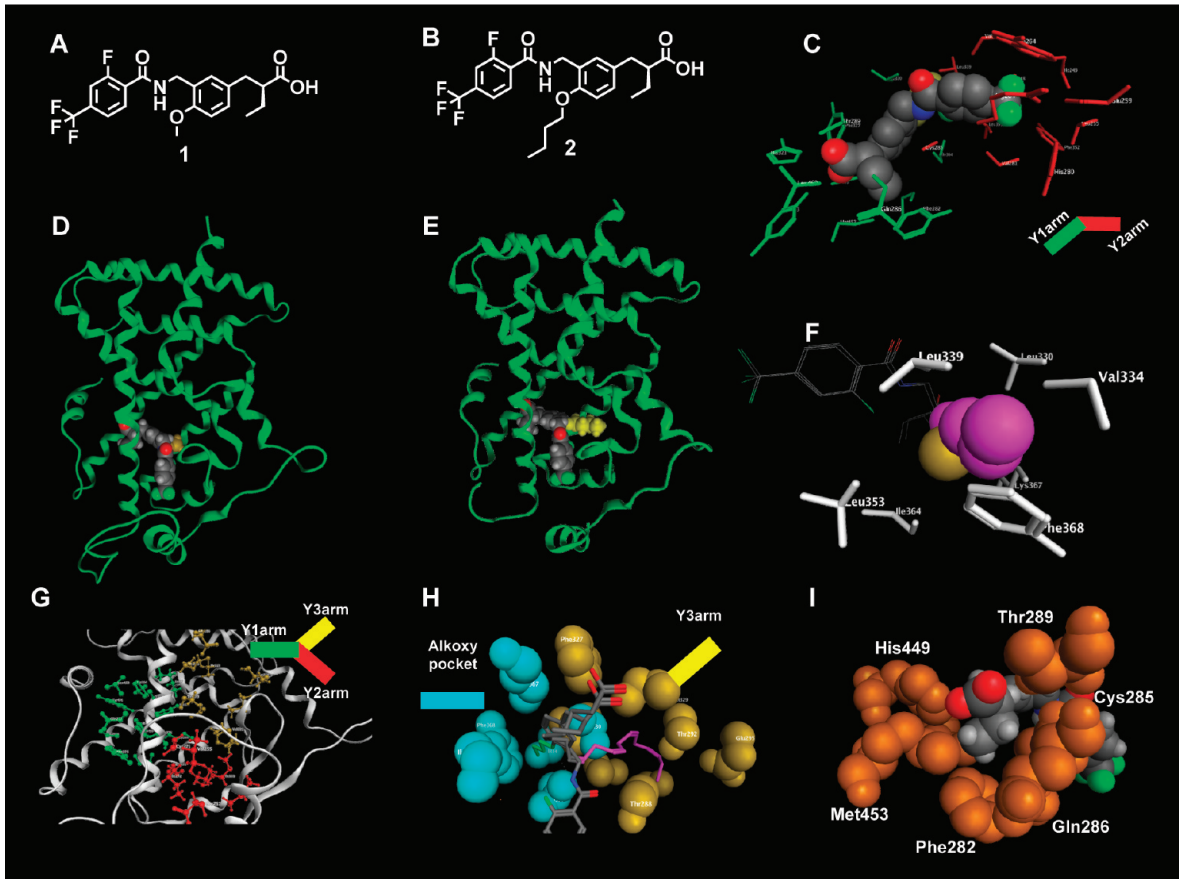

Figure 3. (A) Chemical structure of hPPARα/δ dual agonist (**1**). (B) Chemical structure of hPPARδ-selective agonist (**2**). (C) Zoomed view of the binding mode of **2** in the Y1−Y2 arms. The Y1 arm amino acids and Y2 arm amino acids are depicted as green and red cylinder models, respectively. **2** is depicted as a space-filling model. (D) PPARδ LBD−**1** complex. Protein is represented as a green ribbon model, and the ligand is depicted as a space-filling model. The methoxy group of **1** is highlighted in yellow. (E) PPARδ LBD−**2** complex. The protein is represented as a green ribbon model, and the ligand is depicted as a space-filling model. The butoxy group of **2** is highlighted in yellow. (F) Zoomed view of the amino acids interacting with the alkoxy group of **1** and **2**. The side chain amino acids are depicted as white cylinder models. (G) Zoomed view of the Y-shaped ligand-binding pocket of hPPARδ LBD. Protein is represented as a white ribbon model and the Y1, Y2, and Y3 arm amino acids are depicted as green, red, and yellow ball-and-stick models, respectively. (H) Zoomed view of the structure of the alkoxy pocket and the Y3 arm. The amino acids which form the alkoxy pocket and Y3 arm are depicted as cyan and yellow space-filling models, respectively. (I) Zoomed view of the amino acids interacting with the α-alkyl group of **1**. The side-chain amino acids and the ligand are depicted as space-filling models.

alkoxy side chains are directed not to the Y3 arm but to a small pocket formed by the side-chain amino acids of Leu330, Val334, Leu339, Ile364, Lys367, and Phe368 located just adjacent to the entrance of the Y3 arm. We designate this region of interaction as the alkoxy pocket.

It is noteworthy that the length of the side-chain alkyl group introduced at the α-position of the carboxyl group of this series is critical to determine the potency of the hPPARδ agonistic activity. For example, α-ethyl derivative (**1**) exhibited potent hPPARδ agonistic activity, while the α-*n*-propyl derivative (**5**) exhibited somewhat decreased hPPARδ agonistic activity (of course, the potency of these two compounds cannot be compared quantitatively, because **1** is optically active, while **5** is a racemate, and the introduction of a fluorine atom at the hydrophobic tail part improves both the hPPARα and hPPARδ agonistic activities, as reported previously[14]). The X-ray crystallographic structure of **1** complexed with hPPARδ LBD indicated that the side-chain ethyl group is located in a small cavity composed of bulky amino acids Phe282, Gln286, Thr289, Ile363, Met453, and His449 (Figure 3I). The distances between the terminal methyl group of the α-position ethyl group and Phe282, Ile363, and Met453 were all within 2.5 Å. Therefore, there might not be enough space to accommodate an additional methyl group (i.e., the *n*-propyl group), which might interfere sterically with the surrounding residues, particularly with the side chains of the Phe282, Ile363, and Met453 residues.

We have also solved and reported the X-ray crystallographic structure of hPPAR−pan agonist (**3**) complexed with hPPARα LBD at 3.0 Å resolution. Recently, we also solved the structure of fluorescent hPPARα/δ−dual agonist (**4**) complexed with hPPARα LBD at 1.75 Å resolution. These results are depicted in Figure 4D and E. Similarly to **1** and **2** complexed with hPPARδ LBD, the acidic head part of **3** and **4** is located in the Y1 arm, forming a hydrogen bonding network to Tyr314, His440, and Tyr464, and the hydrophobic tail part is buried in the Y2 arm of the hPPARα LBD (Figure 4C and G). The alkoxy chain of both **3** and **4** is directed toward both the alkoxy pocket and the Y3 arm.

Our previous findings indicated that α-alkylphenypropanoic acid hPPAR agonists bind to hPPARα LBD and hPPARδ LBD with similar conformations; that is, the α-alkylphenylpropanoic acid moiety forms a hydrogen bonding network with the Y1 arm, while the hydrophobic tail part lies in the Y2 arm, and the

dx.doi.org/10.1021/jm2014293 | *J. Med. Chem.* 2012, 55, 893−902

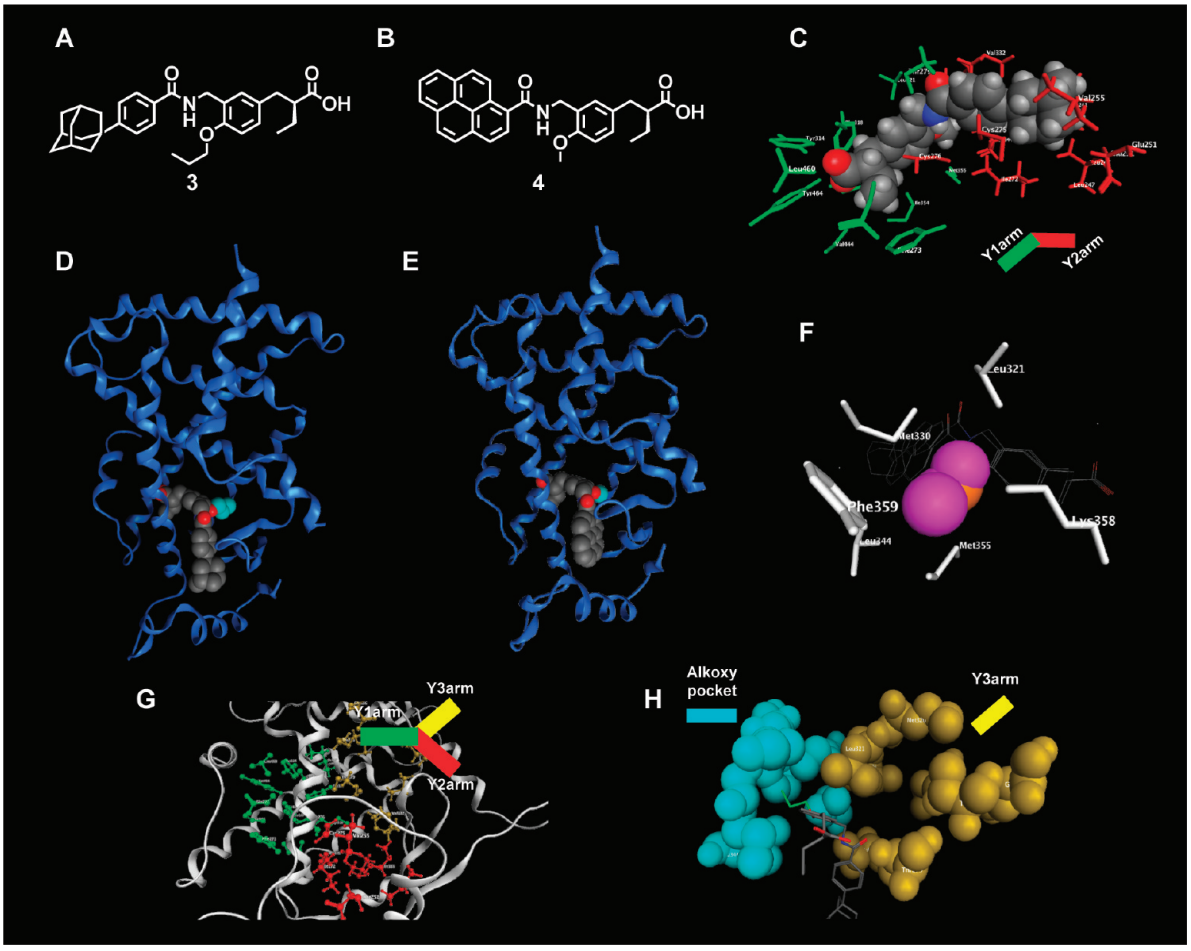

Figure 4. (A) Chemical structure of hPPARα/δ dual agonist (**3**). (B) Chemical structure of hPPAR$\alpha/\delta/\gamma$ pan agonist (**4**). (C) Zoomed view of the binding mode of **4** in the Y1−Y2 arms. The Y1 arm amino acids and Y2 arm amino acids are depicted as green and red cylinder models, respectively. **4** is depicted as a space-filling model. (D) hPPARα LBD−**3** complex. Protein is represented as a blue ribbon model, and the ligand is depicted as a space-filling model. The propoxy group of **3** is highlighted in cyan. (E) hPPARα LBD−**4** complex. The protein is represented as a blue ribbon model, and the ligand is depicted as a space-filling model. The methoxy group of **4** is highlighted in cyan. (F) Zoomed view of the amino acids interacting with the alkoxyl group of **3** and **4**. The side chain amino acids are depicted as white cylinder models. (G) Zoomed view of the Y-shaped ligand-binding pocket of hPPARα LBD. The protein is represented as a white ribbon model, and the Y1 arm, Y2 arm, and Y3 arm amino acids are depicted as green, red, and yellow ball-and-stick models, respectively. (H) Zoomed view of the structure of the alkoxy pocket and the Y3 arm. The amino acids which form the alkoxy pocket and Y3 are depicted as cyan and yellow space-filling models, respectively.

alkoxy side chain at the center benzene ring interacts with the alkoxy pocket located adjacent to the entrance of the Y3 arm.

We anticipated that subtype-selective hPPARγ agonists with the α-alkylphenylpropanoic acid framework as a common scaffold would also bind to hPPARγ LBD in the same conformation as those of **1**, **2** and **3**, **4** complexed with hPPARα LBD and hPPARδ LBD, respectively. *However, this proved not to be the case*, as depicted in Figure 5. Figure 5D and E show the overall structures of (*S*)-2-(4-methoxy-3-((4-(trifluoromethyl)benzamido)methyl)benzyl)pentanoic acid (**5**) and (*S*)-2-(3-((4-(1-adamantyl)benzamido)methyl)-4-(butoxy)benzyl)butanoic acid (**6**) complexed with hPPARγ LBD, respectively. This LBD has a Y-shaped ligand binding pocket (Figure 5C), and the acidic head part of **5** and **6** lies in the Y1 arm, forming a hydrogen-bonding network to Ser289, His323, Tyr327, and Tyr473. The hydrophobic tail part is located in the Y2 arm (Figure 5F). However, the direction of the alkoxy groups of **5** and **6** is completely different from those of **1**, **2** and **3**, **4** complexed with hPPARα LBD and hPPARδ LBD, respectively. Parts G and H of Figure 5 show superimposed structures of **5** and **1** complexed with hPPARγ LBD and hPPARδ LBD, respectively. In Figure 5G, the acidic head parts of **5** and **1** overlap well, but the central benzene rings overlap only poorly. The central benzene ring of **5** is shifted by a distance equivalent to one benzene ring, compared to the position in the case of **1**. The hydrophobic tail parts showed little overlap. The most significant difference between the binding modes of **1** and **5** is the position of the methoxy group at the central benzene ring. The methoxy groups of **1** and **5** lie in opposite directions. In the case of **6** and **3** complexed with hPPARγ LBD and hPPARα LBD, respectively, similar conformations were found, and the acidic head parts and the hydrophobic tail parts overlapped well. However, the central benzene ring is completely flipped, and the butoxy group of **6** and the propoxy group of **3** lie in opposite directions. These structural biological studies clearly indicate that the present α-alkylphenylpropanoic acid derivatives bind to hPPARγ LBD in different conformations, independently of the alkoxy chain length on the central benzene ring and the length of the alkyl chain at the α-position of the carboxyl group, as compared to the binding modes of structurally similar compounds to either hPPARα LBD or hPPARδ LBD. The binding pocket hosting

dx.doi.org/10.1021/jm2014293 | *J. Med. Chem.* 2012, 55, 893−902

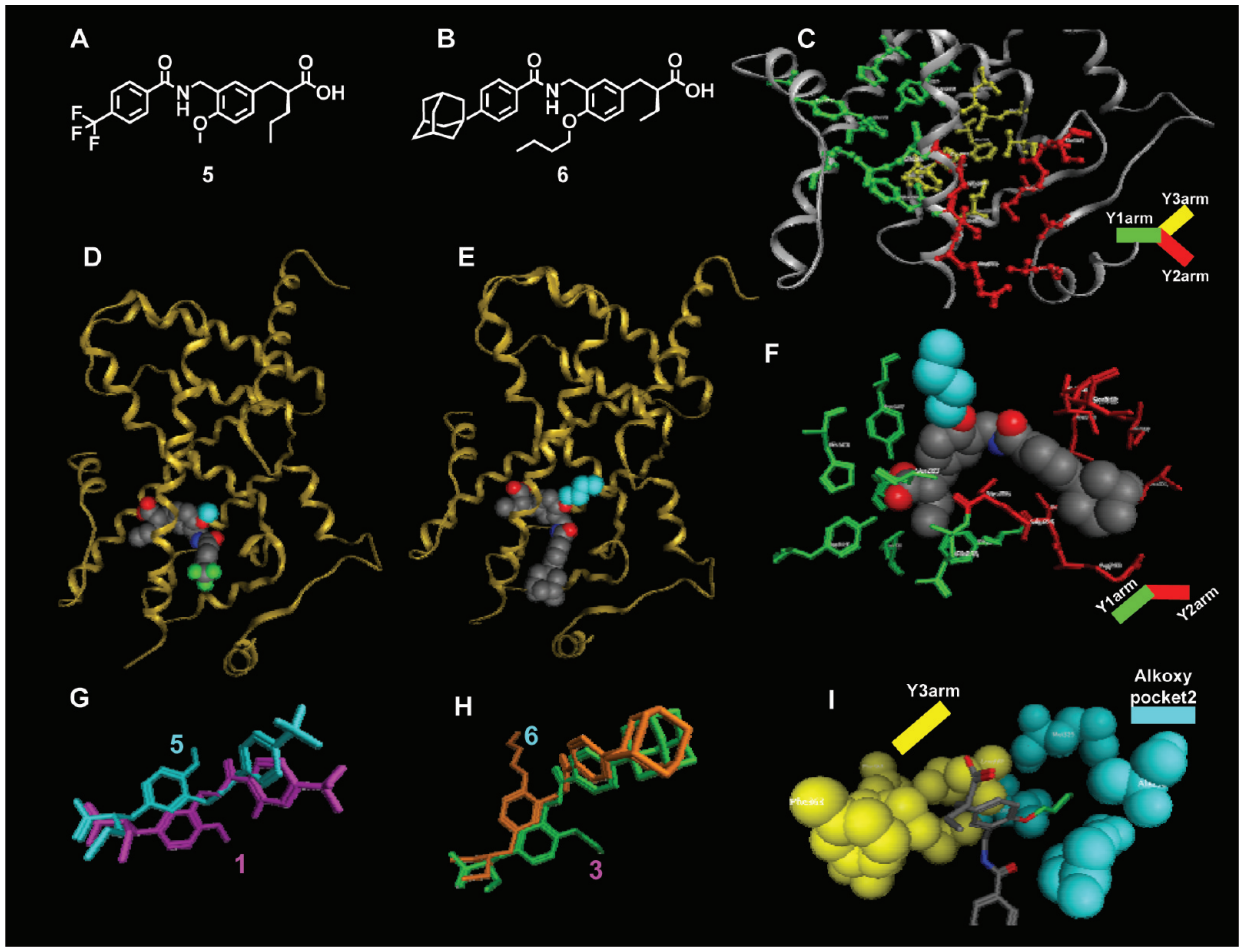

Figure 5. (A) Chemical structure of hPPARγ agonist (**5**). (B) Chemical structure of hPPARγ agonist (**6**). (C) Zoomed view of the Y-shaped ligand-binding pocket of hPPARα LBD. Protein is represented as a white ribbon model, and the Y1, Y2, and Y3 arm amino acids are depicted as green, red, and yellow ball-and-stick models, respectively. (D) hPPARγ LBD−**5** complex. Protein is represented as a yellow ribbon model, and the ligand is depicted as a space-filling model. The methoxy group of **5** is highlighted in cyan. (E) hPPARα LBD−**6** complex. Protein is represented as a blue ribbon model, and the ligand is depicted as a space-filling model. The butoxy group of **6** is highlighted in cyan. (F) Zoomed view of the binding mode of **6** in the Y1−Y2 arms. The Y1 arm amino acids and Y2 arm amino acids are depicted as green and red cylinder models, respectively. **6** is depicted as a space-filling model. (G) The superimposed structures of **1** and **5** complexed with hPPARδ LBD and hPPARγ LBD, respectively. **1** and **5** are depicted as magenta and cyan cylinder models, respectively. (H) The superimposed structures of **3** and **6** complexed with hPPARα LBD and hPPARγ LBD, respectively. **3** and **6** are depicted as green and orange cylinder models, respectively. (I) Zoomed view of the structure of alkoxy pocket 2 and the Y3 arm. The amino acids which form alkoxy pocket 2 and the Y3 arm are depicted as cyan and yellow space-filling models, respectively.

the alkoxy chain is not the alkoxy pocket described above, but another pocket located on the other side of the Y3 arm, composed of the side chains of Pro227, Leu228, Arg288, Glu295, Ile326, Met329, and Leu336. We designate this pocket as alkoxy pocket 2.

2.7. Structural Basis for the Difference of α-Alkylphenylpropanoic Acid Derivative Binding to hPPARγ LBD, as Compared to hPPARα LBD and hPPARδ LBD. In order to understand these discrepancies, we analyzed the binding modes of **1** and **5** complexed with hPPARγ LBD and hPPARδ LBD, respectively. The results are depicted in Figure 6. In the case of the hPPARδ LBD−**1** complex, Thr288 is located close to the carbonyl oxygen of the linker part of **1**, with a hydrogen-bonding interaction between the carbonyl oxygen and the hydrogen of the side chain hydroxy group of Thr288. Therefore, the carbonyl group of **1** is bent toward H3. As a result, the hydrophobic tail part of **1** is removed from H3 and makes hydrophobic contact with the surrounding amino acid residues (Figure 6A and B). In the case of hPPARα LBD, the amino acid 288 is also threonine, and the carbonyl oxygen of **3** and **4** has a hydrogen-bonding interaction with Thr288.

However, in the case of hPPARγ LBD, the amino acid 288 is not threonine but is the basic amino acid arginine. No interaction between the carbonyl oxygen of the linker part of **5** and the side chain of Arg288 was observed. As a result, the carbonyl group of **5** is bent away from H3. The hydrophobic tail part of **5** then makes hydrophobic contact with the surrounding amino acid residues (Figure 6B and C).

We next focused on the side-chain methyl group of Thr288. In the case of the hPPARδ LBD−**1** complex, the side-chain methyl group of Thr288 makes hydrophobic contact with one of the methylene hydrogens of the linker part of **1**, and the distance between the methyl side chain of Thr288 and the methylene hydrogen of **1** is only 3 Å.[26] There is not enough space to allow interaction with the side-chain methoxy group of **1** by flipping to the Thr288 side, so the methoxy group of **1** is placed opposite to the Thr288 side to avoid a steric clash (Figure 6D). Figure 6E is a zoomed view of **5** computationally

dx.doi.org/10.1021/jm2014293 | J. Med. Chem. 2012, 55, 893−902

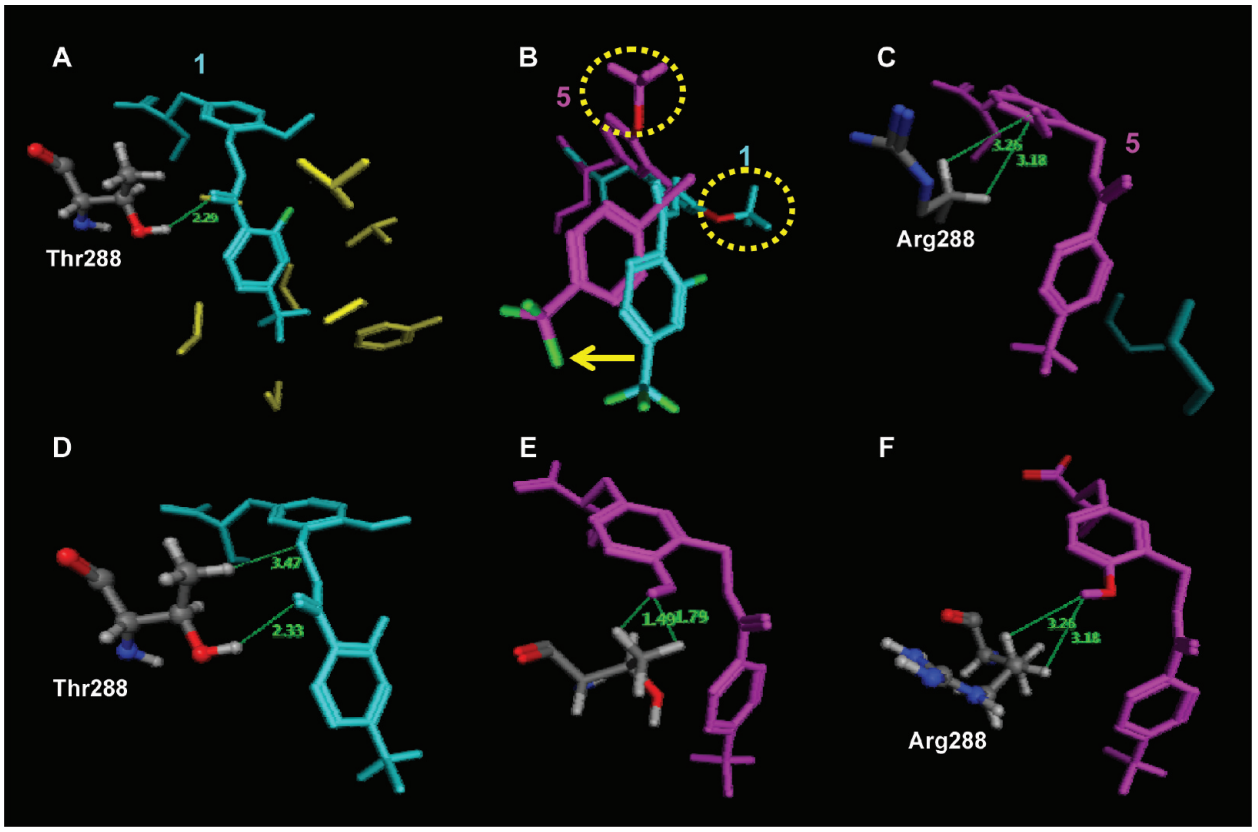

Figure 6. (A) Zoomed view of the amino acids interacting with the hydrophobic tail part of **1**. The side-chain amino acids are depicted as yellow cylinder models. The hydrogen-bonded Thr288 is highlighted. The ligand is depicted as a cyan cylinder model. (B) The superimposed structures of **1** and **5** complexed with hPPARδ LBD and hPPARγ LBD, respectively. **1** and **5** are depicted as magenta and cyan cylinder models, respectively. The methoxy group of each of them is highlighted as a yellow dashed circle. The yellow arrow indicated the shift of the hydrophobic tail part of **5** toward H3. (C) Zoomed view of the amino acids interacting with the hydrophobic tail part of **5**. The side-chain amino acids are depicted as cyan cylinder models. Arg288 is highlighted. The ligand is depicted as a magenta cylinder model. (D) Zoomed view of **1** interacting with Thr2888 of the hPPARδ LBD. A hydrogen-bonding interaction is apparent between the carbonyl oxygen of **1** and the hydroxyl group of Thr288. (E) Superimposed structure of **5** complexed with hPPARγ LBD. The methoxy group of **5** interferes sterically with the side-chain methyl group of Thr288. (F) Zoomed view of **5** interacting with Arg288 on hPPARγ LBD. Hydrophobic interaction is apparent between the methoxy group of **5** and the methylene part of Arg288.

superimposed on the hPPARδ LBD to check the distance between the methyl side chain of Thr288 and the methylene hydrogen of **5**. In the case of **5** complexed with hPPARγ LBD, however, Arg288 has a long but slim side chain, so the central benzene ring of **5** can rotate, allowing the methoxy group on the central benzene ring to make hydrophobic contact with the side-chain methylene group of Arg288.

2.8. Structural Basis for Improvement of hPPARγ Agonistic Activity by the Adamantyl Group at the Hydrophobic Tail Part. As reported previously, we have found that the steric bulkiness of the substituent introduced at the hydrophobic tail part of compounds in the present series is correlated with the hPPARγ agonistic activity, and we have shown that the adamantyl group is an effective substituent for hPPARγ agonists.[16] However, the exact reason was not established. The present structural biology study results clearly explain why the activity toward hPPARγ is improved by the introduction of the three dimensionally bulky adamantyl groups. Figure 7A–C shows the hPPARs LBD structures, and it can be seen that the amino acids forming the entry to the hydrophobic cavity, comprising Ile249, Ile262, Glu259, Arg280, Ile281, Gly284, and Ile341, host the hydrophobic tail part of the present series of compounds. In the case of hPPARδ LBD, these amino acids are Trp264 located on the H3 helix and Arg284 located on the omega loop, while the corresponding amino acids of hPPARα LBD and hPPARγ LBD are Cys275, Leu254 and Gly284, Ile249, respectively. The width of the entry leading to the hydrophobic cavity is on the order of hPPARγ LBD > hPPARα LBD > hPPARδ LBD (Figure 7D). Thus, the hydrophobic cavity hosting the hydrophobic tail part is widest in hPPARγ LBD among the three subtypes. In the case of **5**, the trifluoromethyl group may not be large enough for effective hydrophobic interaction with the cavity (Figure 7E), whereas, in the case of **6**, the adamantyl group can interact well with the cavity, especially the side chains of Ile249, Ile262, Arg280, and Ile281 (Figure 7F; these amino acids are highlighted as magenta space-filling models).

In summary, we have solved the X-ray crystallographic structures of the hPPARα LBD–**4** complex, the hPPARγ LBD–**5** complex, and the hPPARγ LBD–**6** complex at 1.75 Å, 2.2 Å, and 2.6 Å resolutions, respectively. In contrast to the previously solved structures of the structurally similar compounds **1**–**3** complexed with either hPPARδ LBD or hPPARα LBD, compounds **5** and **6** bind to hPPARγ LBD with distinctly different conformations. Although the hPPAR subtypes share 65–80% identity, and the present series of α-alkylphenylpropanoic acid hPPAR agonists are all structurally closely similar, there are distinct binding mode differences among the hPPAR subtypes. Medicinal chemists often expect that a series of compounds with the same basic framework

dx.doi.org/10.1021/jm2014293 | J. Med. Chem. 2012, 55, 893–902

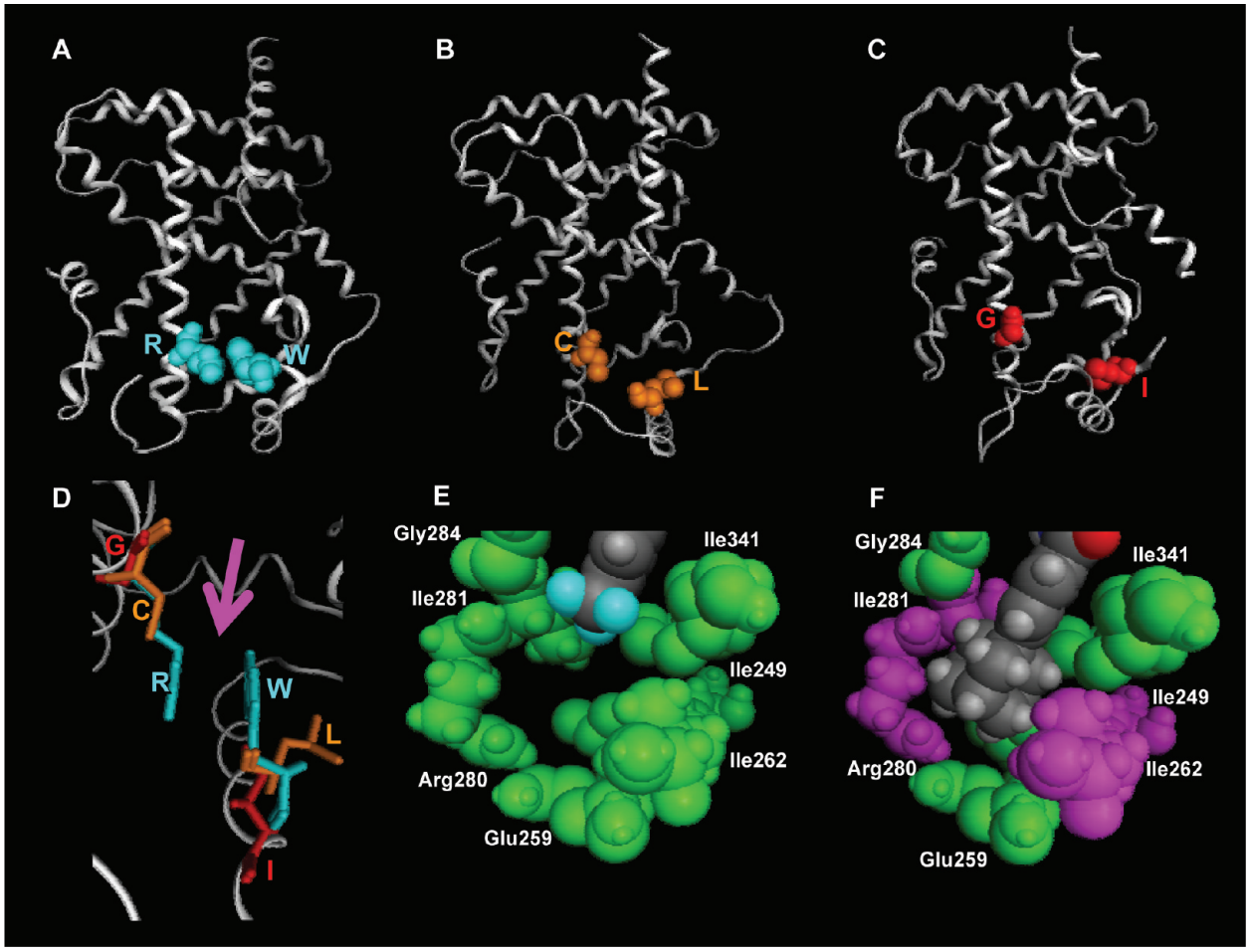

Figure 7. (A) Whole structure of the hPPARδ LBD−**4** complex. The structure of **4** is omitted, and the important amino acids which regulate the entry of the hydrophobic tail part of **4** are highlighted as a blue space-filling model. (B) Whole structure of the hPPARγ LBD−**5** complex. The structure of **5** is omitted, and the important amino acids which regulate the entry of the hydrophobic tail part of **5** are highlighted as an orange space-filling model. (C) Whole structure of the hPPARγ LBD−**6** complex. The structure of **6** is omitted, and the important amino acids which regulate the entry of the hydrophobic tail part of **6** are highlighted as a red space-filling model. (D) Zoomed view of the aligned structures of a hPPARα LBD, a hPPARδ LBD, and a hPPARγ LBD. The entranced amino acids of a hPPARα LBD, a hPPARδ LBD, and a hPPARγ LBD were expressed as blue, orange, and red cylinder models, respectively. (E) Zoomed view of the amino acids interacting with the hydrophobic tail part of **5** complexed with hPPARγ LBD. The side chain amino acids and the ligand are depicted as space-filling models. (F) Zoomed view of the amino acids interacting with the hydrophobic tail part of **6** complexed with hPPARγ LBD. The side chain amino acids and the ligand are depicted as space-filling models.

would bind to structurally related receptors and/or enzymes in the same conformation. However, the present results show that this is not necessarily the case. To avoid misunderstanding of structure−activity relationship results, it is important to consider the results of X-ray crystallographic analysis, instead of default use of currently available computational software.

3. EXPERIMENTAL SECTION

Chemistry. General Methods. Melting points were determined with a Yanagimoto hot-stage melting point apparatus and are uncorrected. NMR spectra were recorded on a VarianVXR-300 (^{1}H-300 MHz) spectrometer. Proton chemical shifts were referenced to TMS as an internal standard. Elemental analysis was carried out with a Yanagimoto MT-5 CHN recorder elemental analyzer, and results were within 0.4% of the theoretical values. FAB-MS was carried out with a VG70-SE.

*3.1.1. 2-(4-Methoxy-3-((4-(trifluoromethyl)benzamido)methyl)-benzyl)pentanoic Acid (Racemic **5**).* The physicochemical properties of this compound are as follows: ^{1}H NMR (300 MHz, $CDCl_3$) δ 7.85 (d, J = 8.1 Hz, 2H), 7.66 (d, J = 8.1 Hz, 2H), 7.16 (d, J = 1.8 Hz, 1H), 7.10 (dd, J = 8.1 Hz, 2.2 Hz, 1H), 6.82−6.78 (m, 2H), 4.58 (d, J = 5.9 Hz, 2H), 3.85 (s, 2H), 2.91−2.83 (m, 1H), 2.74−2.59 (m, 2H), 1.70−1.56 (m, 1H), 1.53−1.28 (m, 3H), 0.90 (t, J = 7.4 Hz, 3H); HRMS (FAB, $(M + H)^+$) calcd for $C_{23}H_{24}F_3NO_5$ 424.1720, found 424.1719; HPLC purity was estimated to be 97.2% by means of reversed-phase HPLC, using a Pegasil ODS sp100 column (4.6 mm × 250 mm, Senshu Chemical, Japan) fitted on a Shimadzu HPLC system, with CH_3CN:0.1% TFA = 3:1 v/v as the eluant and with detection at 254 nm.

*3.1.2. 2-(3-((4-(1-Adamantyl)benzamido)methyl)-4-(butoxy)-benzyl)butanoic Acid (Racemic **6**).* The physicochemical properties of this compound are as follows: ^{1}H NMR (300 MHz, $CDCl_3$) δ 7.70 (d, J = 8.8 Hz, 2H), 7.40 (d, J = 8.8 Hz, 2H), 7.16 (d, J = 2.2 Hz, 1H), 7.16 (dd, J = 8.8 Hz, 2.2 Hz, 1H), 6.79−6.71 (m, 2H), 4.59 (d, J = 5.9 Hz, 2H), 3.99 (t, J = 6.6 Hz, 2H), 2.90−2.83 (m, 1H), 2.74−2.67 (m, 1H), 2.58−2.53 (m, 1H), 2.10 (brs, 3H), 1.90 (brs, 6H), 1.82−1.47 (m, 12H), 1.00−0.92 (m, 6H); HRMS (FAB, $(M + H)^+$) calcd for $C_{33}H_{43}NO_4$ 518.3270, found 518.3255; Anal. ($C_{33}H_{43}NO_4 \cdot {}^1/_2H_2O$) C, H, N.

HPLC purity was estimated to be 96.7% by means of reversed phase-HPLC, using a Pegasil ODS sp100 column (4.6 mm × 250 mm, Senshu Chemical, Japan) fitted on a Shimadzu HPLC system, with CH_3CN:0.1% TFA = 4:1 v/v as the eluant and detection at 254 nm.

dx.doi.org/10.1021/jm2014293 | J. Med. Chem. 2012, 55, 893−902

■ ASSOCIATED CONTENT

PDB ID codes

3VI8, hPPARα LBD−**4**; 3VJH, hPPARγ LBD−**5**; 3VJI, hPPARγ LBD−**6**

■ AUTHOR INFORMATION

Corresponding Author

*E-mail: miyachi@pharm.okayama-u.ac.jp. Telephone: +81-086-251-7930.

Author Contributions

†These authors contributed equally to this work.

■ ACKNOWLEDGMENTS

This work was supported in part by the Targeted Proteins Research Program of the Japan Science and Technology Corporation (JST), the Uehara Memorial Foundation, and the Tokyo Biochemical Research Foundation (TBRF).

■ ABBREVIATIONS USED

NR, nuclear receptor; hPPAR, human peroxisome proliferator-activated receptor; LBD, ligand-binding domain; PDB, protein data bank

■ REFERENCES

(1) Chawla, A.; Repa, J. J.; Evans, R. M.; Mangelsdorf, D. J. Nuclear receptors and lipid physiology: Opening the X-files. *Science* **2001**, *294*, 1866−1870.

(2) Lemberger, T.; Desvergne, B.; Wahli, W. Peroxisome proliferator-activated receptors: a nuclear receptor signaling pathway in lipid physiology. *Annu. Rev. Cell Dev. Biol.* **1996**, *12*, 335−363.

(3) Banner, C. D.; Göttlicher, M.; Widmark, E.; Sjövall, J.; Rafter, J. J.; Gustafsson, J. A Systematic analytical chemistry/cell assay approach to isolate activators of orphan nuclear receptors from biological extracts: characterization of peroxisome proliferator-activated receptor activators in plasma. *J. Lipid Res.* **1993**, *34*, 1583−1591.

(4) Schoonjans, K.; Martin, G.; Staels, B.; Auwerx, J. Peroxisome proliferator-activated receptors, orphans with ligands and functions. *Curr. Opin. Lipidol.* **1997**, *8*, 159−166.

(5) Mendez, M.; LaPointe, M. C. PPARgamma inhibition of cyclooxygenase-2, PGE2 synthase, and inducible nitric oxide synthase in cardiac myocytes. *Hypertension* **2003**, *42*, 844−850.

(6) Morrison, R. F.; Farmer, S. R. Role of PPARgamma in regulating a cascade expression of cyclin-dependent kinase inhibitors, p18-(INK4c) and p21(Waf1/Cip1), during adipogenesis. *J. Biol. Chem.* **1999**, *274*, 17088−17097.

(7) Huang, J. W.; Shiau, C. W.; Yang, J.; Wang, D. S.; Chiu, H. C.; Chen, C. Y.; Chen, C. S. Development of small-molecule cyclin D1-ablative agents. *J. Med. Chem.* **2006**, *49*, 4684−4689.

(8) Wang, N.; Yin, R.; Liu, Y.; Mao, G.; Xi, F. Role of peroxisome proliferator-activated receptor-γ in atherosclerosis: an update. *Circ. J.* **2011**, *75*, 528−535.

(9) Kaundal, R. K.; Sharma, S. S. Peroxisome proliferator-activated receptor gamma agonists as neuroprotective agents. *Drug News Perspect.* **2010**, *23*, 241−256.

(10) Landreth, G. Therapeutic use of agonists of the nuclear receptor PPARgamma in Alzheimer's disease. *Curr. Alzheimer Res.* **2007**, *4*, 159−164.

(11) Xu, H. E.; Stanley, T. B.; Montana, V. G.; Lambert, M. H.; Shearer, B. G.; Cobb, J. E.; McKee, D. D.; Galardi, C. M.; Plunket, K. D.; Nolte, R. T.; Parks, D. J.; Moore, J. T.; Kliewer, S. A.; Willson, T. M.; Stimmel, J. B. Structural basis for antagonist-mediated recruitment of nuclear co-repressors by PPARalpha. *Nature (London)* **2002**, *415*, 813−817.

(12) (a) Cronet, P.; Petersen, J. F.; Folmer, R.; Blomberg, N.; Sjoblom, K.; Karlsson, U.; Lindstedt, E. L.; Bamberg, K. Structure of the PPARalpha and -gamma ligand binding domain in complex with AZ 242; ligand selectivity and agonist activation in the PPAR family. *Structure* **2001**, 699−706. (b) Stanley, T. B.; Leesnitzer, L. M.; Montana, V. G.; Galardi, C. M.; Lambert, M. H.; Holt, J. A.; Xu, H. E.; Moore, L. B.; Blanchard, S. G.; Stimmel, J. B. Subtype specific effects of peroxisome proliferator-activated receptor ligands on corepressor affinity. *Biochemistry* **2003**, *42*, 9278−9287. (c) Ostberg, T.; Svensson, S.; Selén, G.; Uppenberg, J.; Thor, M.; Sundbom, M.; Sydow-Bäckman, M.; Gustavsson, A. L.; Jendeberg, L. A new class of peroxisome proliferator-activated receptor agonists with a novel binding epitope shows antidiabetic effects. *J. Biol. Chem.* **2004**, *279*, 41124−30. (d) Ambrosio, A. L.; Dias, S. M.; Polikarpov, I.; Zurier, R. B.; Burstein, S. H.; Garratt, R. C. Ajulemic acid, a synthetic nonpsychoactive cannabinoid acid, bound to the ligand binding domain of the human peroxisome proliferator-activated receptor gamma. *J. Biol. Chem.* **2007**, *282*, 18625−18633. And others cited in these references.

(13) Ban, S.; Kasuga, J.; Nakagome, I.; Nobusada, H.; Takayama, F.; Hirono, S.; Kawasaki, H.; Hashimoto, Y.; Miyachi, H. Structure-based design, synthesis, and nonalcoholic steatohepatitis (NASH)-preventive effect of phenylpropanoic acid peroxisome proliferator-activated receptor (PPAR) α-selective agonists. *Bioorg. Med. Chem.* **2011**, *19*, 3183−3191.

(14) Kasuga, J.; Yamasaki, D.; Araya, Y.; Nakagawa, A.; Makishima, M.; Doi, T.; Hashimoto, Y.; Miyachi, H. Design, synthesis and evaluation of a novel series of α-substituted phenylpropanoic acid derivatives as human peroxisome proliferator-activated receptor (PPAR) alpha/delta dual agonists for the treatment of metabolic syndrome. *Bioorg. Med. Chem.* **2006**, *14*, 8405−8414.

(15) Kasuga, J.; Nakagome, I.; Aoyama, A.; Sako, K.; Ishizawa, M.; Ogura, M.; Makishima, M.; Hirono, S.; Hashimoto, Y.; Miyachi, H. Design, synthesis, and evaluation of potent, structurally novel peroxisome proliferator-activated receptor (PPAR) delta-selective agonists. *Bioorg. Med. Chem.* **2007**, *15*, 5177−5190.

(16) Kasuga, J.; Yamasaki, D.; Ogura, K.; Shimizu, M.; Sato, M.; Makishima, M.; Doi, T.; Hashimoto, Y.; Miyachi, H. SAR-oriented discovery of peroxisome proliferator-activated receptor pan agonist with a 4-adamantylphenyl group as a hydrophobic tail. *Bioorg. Med. Chem. Lett.* **2008**, *18*, 1110−1105.

(17) Ohashi, M.; Oyama, T.; Nakagome, I.; Sato, M.; Nishio, Y.; Nobusada, H.; Hirono, S.; Morikawa, K.; Hashimoto, Y.; Miyachi, H. Design, synthesis, and structural analysis of phenylpropanoic acid-type PPARγ-selective agonists: Discovery of reversed stereochemistry—activity relationship. *J. Med. Chem.* **2011**, *54*, 331−341.

(18) Oyama, T.; Toyota, K.; Waku, T.; Hirakawa, Y.; Nagasawa, N.; Kasuga, J.; Hashimoto, Y.; Miyachi, H.; Morikawa, K. Adaptability and selectivity of human peroxisome proliferator-activated receptor (PPAR) pan agonists revealed from crystal structures. *Acta Crystallogr., D: Biol. Crystallogr.* **2009**, *65*, 786−795.

(19) Kasuga, J.; Oyama, T.; Hirakawa, Y.; Makishima, M.; Morikawa, K.; Hashimoto, Y.; Miyachi, H. Improvement of the transactivation activity of phenylpropanoic acid-type peroxisome proliferator-activated receptor pan agonists: effect of introduction of fluorine at the linker part. *Bioorg. Med. Chem. Lett.* **2008**, *18*, 4525−4528.

(20) Kasuga, J.; Oyama, T.; Nakagome, I.; Makishima, M.; Hirono, S.; Morikawa, K.; Hashimoto, Y.; Miyachi, H. Determination of the critical amino acids involved in the peroxisome proliferator-activated receptor (PPAR) delta selectivity of phenylpropanoic acid-derived agonists. *ChemMedChem* **2008**, *3*, 1662−1666.

(21) Brunger, A. T.; Adams, P. D.; Clore, G. M.; DeLano, W. L.; Gros, P.; Grosse-Kunstleve, R. W.; Jiang, J.-S.; Kuszewski, J.; Nilges, M.; Pannu, N. S.; Read, R. J.; Rice, L. M.; Simonson, T.; Warren, G. L. Crystallography & NMR system: A new software suite for macromolecular structure determination. *Acta Crystallogr.* **1998**, *D54*, 905−921.

(22) Jones, T. A.; Zou, J.-Y.; Cowan, S. W.; Kjeldgaard, M. Improved methods for building protein models in electron density maps and the location of errors in these models. *Acta Crystallogr.* **1991**, *A47*, 110−119.

(23) Kleywegt, G. J. Crystallographic refinement of ligand complexes. *Acta Crystallogr.* **2007**, *D63*, 94−100.
(24) Fetrow, J. S. Omega loops: nonregular secondary structures significant in protein function and stability. *FASEB J.* **1995**, *9*, 708−717.
(25) Xu, H, E.; Lambert, M. H.; Montana, V. G.; Parks, D. J.; Blanchard, S. G.; Brown, P. J.; Sternbach, D. D.; Lehmann, J. M.; Wisely, G. B.; Willson, T. M.; Kliewer, S. A.; Milburn, M. V. Molecular recognition of fatty acids by peroxisome proliferator-activated receptors. *Mol. Cell* **1999**, *3*, 397−403.
(26) Computer-graphic work and hydrogen bonding distances measurement were performed using MOE (Molecular Operating Environment) (Ryoka Systems Inc.).